Image Quality Assessment of Standard- and Low-Dose Chest CT Using Filtered Back Projection, Adaptive Statistical Iterative Reconstruction, and Novel Model-Based Iterative Reconstruction Algorithms

Varut Vardhanabhuti[1,2]
Robert J. Loader[3]
Grant R. Mitchell[1]
Richard D. Riordan[1]
Carl A. Roobottom[1,2]

OBJECTIVE. The purpose of this article is to compare image quality between filtered back projection (FBP), adaptive statistical iterative reconstruction (ASIR), and model-based iterative reconstruction (MBIR) at standard dose and two preselected low-dose scans.

SUBJECTS AND METHODS. Thirty patients (16 men and 14 women; mean age, 67 years) were prospectively recruited. Patients underwent three scans (one standard-dose scan and two low-dose scans at noise indexes [NIs] of 33, 60, and 70, respectively). All three scans were reconstructed with FBP, ASIR, and MBIR. Objective and subjective image qualities were compared. Dose-length products and effective doses for each scans were recorded. Mean image noise and attenuation values were compared between different reconstruction algorithms using repeated-measures analysis of variance and paired Student *t* tests. The interobserver variation between the two radiologists for subjective image quality and lesion assessment was estimated by using weighted kappa statistics.

RESULTS. Objective image analysis supports significant noise reduction with low-dose scans using the MBIR technique ($p < 0.05$). There was no significant change in mean CT numbers between different reconstructions ($p > 0.05$). Subjective analysis reveals no significant difference between image quality and diagnostic confidence between low-dose MBIR scans compared with standard-dose scans reconstructed using ASIR ($p > 0.05$). Average effective doses were 3.7, 1.2, and 0.9 mSv for standard scans at NIs of 33, 60, and 70, respectively.

CONCLUSION. MBIR shows superior noise reduction and improved image quality. Substantial dose reduction can be achieved by increasing the NI parameters as tested in this study without affecting image quality and diagnostic confidence.

Keywords: adaptive statistical iterative reconstruction, CT, iterative reconstruction, model-based iterative reconstruction

DOI:10.2214/AJR.12.9424

Received June 14, 2012; accepted after revision September 7, 2012.

[1]Department of Radiology, Derriford Hospital, Derriford Rd, Plymouth, Devon PL6 8DH, UK. Address correspondence to V. Vardhanabhuti (v.vardhanabhuti@nhs.net).

[2]Plymouth University Peninsula Schools of Medicine and Dentistry, John Bull Building, Plymouth, UK.

[3]Department of Clinical and Radiation Physics, Derriford Hospital, Derriford Rd, Plymouth, UK.

CME/SAM
This article is available for CME/SAM credit.

AJR 2013; 200:545–552

0361–803X/13/2003–545

Medical radiation is the largest source of controllable radiation exposure and it accounts for more than 95% of radiation from artificial sources. The largest cause of medical-related radiation is CT examinations, and the number of examinations is increasing rapidly [1, 2]. A Health Protection Agency publication showed a 28% increase over a 10-year period (from 1997–1998 to 2007–2008) in the United Kingdom [3]. This increase is mainly the result of a doubling of the number of CT examinations. Although CT accounts for only 11% of the examinations, it contributes 68% of the collective dose [1]. Several methods have been developed to reduce the radiation burden related to CT examinations. One promising avenue to tackle this problem relates to scanning at lower dose levels while using novel reconstruction techniques to improve image quality. Recent use of adaptive statistical iterative reconstruction (ASIR) has shown much promise in improving image quality when scanning at a lower dose [4–11]. The next evolution of this iterative reconstruction technique comes in the form of the model-based iterative reconstruction (MBIR), also known as Veo (GE Healthcare).

The purpose of this study is of twofold. First, we compare objective measures of image quality between the traditional reconstruction method of filtered back projection (FBP) with ASIR and MBIR using one standard-dose scan and two low-dose scans (with dose selection based on a previous phantom study). Second, we compare diagnostic confidence of standard-dose FBP and ASIR scans versus low-dose MBIR scans to assess the feasibility of low-dose scanning in clinical practice.

Subjects and Methods

Patient Selection

Our institutional review board and regional ethics committee governing human research approved this prospective clinical study. Informed consent

was obtained from all patients. Patients had to be older than 50 years and had to be scheduled for a standard-of-care chest CT with specific indications (oncologic diagnosis, staging, response to treatment, or posttreatment surveillance). Patients also had to be hemodynamically stable (i.e., respiratory rate of 12–40 breaths/min, pulse rate < 100 beats/min, and systolic blood pressure of 100–140 mm Hg), able to give written informed consent, and able to hold their breath and remain still for 15 seconds at a time. Exclusion criteria include age younger than 50 years, inability to give informed consent, hemodynamic instability, a requirement for multiphasic CT chest examinations, and prior contrast agent reaction. Thirty patients were prospectively recruited (16 men and 14 women). Mean (± SD) weight was 75.7 ± 18.6 kg (range, 41–124 kg). Mean age was 67 ± 9 years (range, 51–84 years). Scans were performed between October 28, 2011, and January 31, 2012.

Scanning Techniques

Scans were performed using a 64-MDCT scanner (Discovery CT750HD, GE Healthcare) with IV administration of 100 mL of contrast agent (ioversol 300; Optiray, Covidien). Scan initiation commenced using a bolus-tracking method with regions of interest (ROIs) drawn over the aorta. All scans were acquired at 1.25-mm slice thickness. Standard-of-care scans were performed first at a noise index (NI) of 33, which is used routinely in our clinical practice. Immediately after the standard-of-care scans, two low-dose scans were performed at NIs of 60 and 70, effectively reducing the tube current delivered to the patient per rotation. To save time, scans were performed in the caudocranial direction after the initial scan, and then in the craniocaudal direction (Fig. 1), without a compulsory delay of 1 second between each phase. All three phases of scanning through the chest were performed within a single breath-hold, to minimize motion and misregistration artifacts and to minimize time delay between acquisitions of research images and the initial standard-of-care contrast-enhanced CT images. To allow potential differences in IV contrast agent opacification, the low-dose scans were acquired in randomized order. All scanning parameters, with the exception of NI (and therefore tube current), were held constant (tube voltage, 120 kVp; pitch, 0.984:1; table speed, 39.37 mm/gantry rotation; helical acquisition mode; detector configuration, 64 × 0.625-mm; gantry rotation time, 0.5 second; reconstructed section thickness, 0.625, 1.25, and 5 mm; reconstructed section interval, 0.625, 1.25, and 5 mm; and standard reconstruction kernel). The tube current range was set to 10–750 mA. This particular scanner allows specific tube current settings of 10 mA minimum and 750 mA maximum.

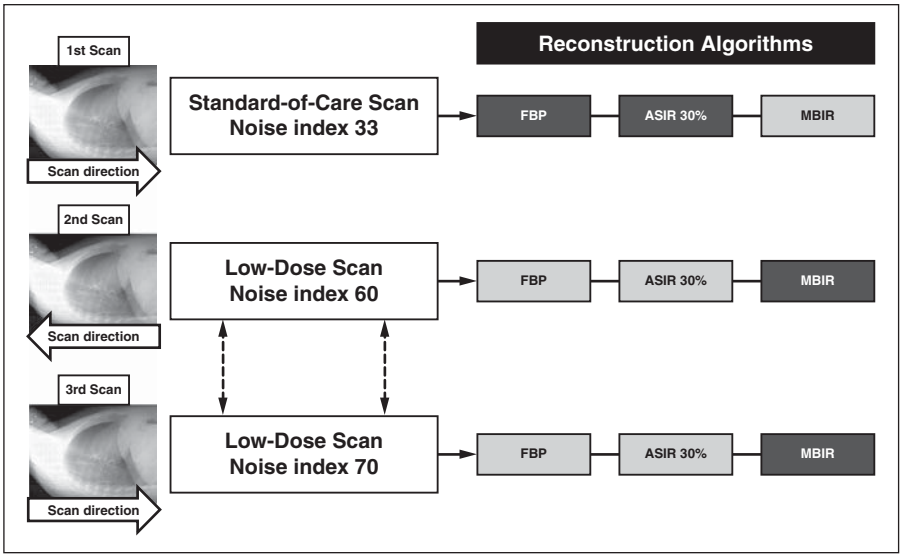

Fig. 1—Scanning parameters and reconstruction methods. Note that standard-of-care scan is always performed in craniocaudal direction. To save time, second scan is done in caudocranial direction, and third scan is done in craniocaudal direction. There is delay of 1 second between each scan. All three scans were performed within single breath-hold (usually around 12–15 seconds). To allow differences in contrast opacification between second and third scans, equal numbers of noise index (NI) 60 and 70 are assigned to second and third scan groups. Each scan is reconstructed in all three reconstruction algorithms. All nine series are used for objective analysis. Only filtered back projection (FBP) at NI 33, adaptive statistical iterative reconstruction (ASIR) at NI 33 (with 30% blending), and model-based iterative reconstruction (MBIR) at NIs 60 and 70 were used for subjective analysis.

Image Reconstruction

All three scans were reconstructed with FBP, ASIR (with 30% blending), and MBIR. The average computing time for MBIR is approximately 50 minutes per series, and it is performed in the background, during which time the scanner can be used to scan other patients. In 30 patients, this resulted in 270 image datasets. All 270 datasets were used to perform objective image analysis. For subjective assessment, the purpose of this study is to compare the diagnostic confidence of low-dose MBIR images with that of standard-dose FBP and ASIR images; therefore, 120 image datasets were created comprising standard-of-care ASIR images at an NI of 33, FBP images at an NI of 33, and low-dose MBIR images at NIs of 60 and 70, which were coded, anonymized, and reconstructed into 1.25- and 5-mm axial sections and 5-mm coronal and sagittal reformats for subjective image analysis. This was done solely by a study author who did not take part in subjective image analysis.

Objective Analysis

Mean objective image noise and CT numbers (both measured in Hounsfield units) were measured for 270 CT image series (1.25-mm slice thickness). ROIs were circular (size, 1–3 cm^2) and drawn on axial planes placed over six anatomic regions. These were as follows: in the subcutaneous fat within the anterior chest wall (left and right) at the level of aortic arch, in the subcutaneous fat within the subaxillary region (left and right), and in the muscle region of paraspinal muscles (left and right) (Fig. 2). Background noise measurements were taken as the SDs in an ROI. Mean attenuation values were also recorded for the six anatomic regions. All scans were loaded at the same time, and care was taken to place ROIs at roughly the same location between image series. This was aided by the use of the propagation function of ROIs across multiple linked series, and, where possible, we avoided areas of inhomogeneity (e.g., small blood vessels). Once all ROIs were performed, these were saved (as "Saved State") and could be retrospectively reloaded to check for inputting errors.

Subjective Analysis

All chest CT image datasets for each patient were viewed side by side on a PACS diagnostic workstation (Nio 3MP, Barco). The order in which each reconstruction method was presented was randomized. Images were available as axial thick (5 mm) and thin (1.25 mm) sections, as well as coronal and sagittal reformats at 5-mm thickness. Two thoracic radiologists (with 12 and 7 years of experience, respectively) assessed all image datasets. Standard mediastinal (window width, 400 HU; window level, 40 HU) and lung parenchymal (window width, 1600 HU; window center, −600 HU) window settings were used for image assessment, but radiologists were

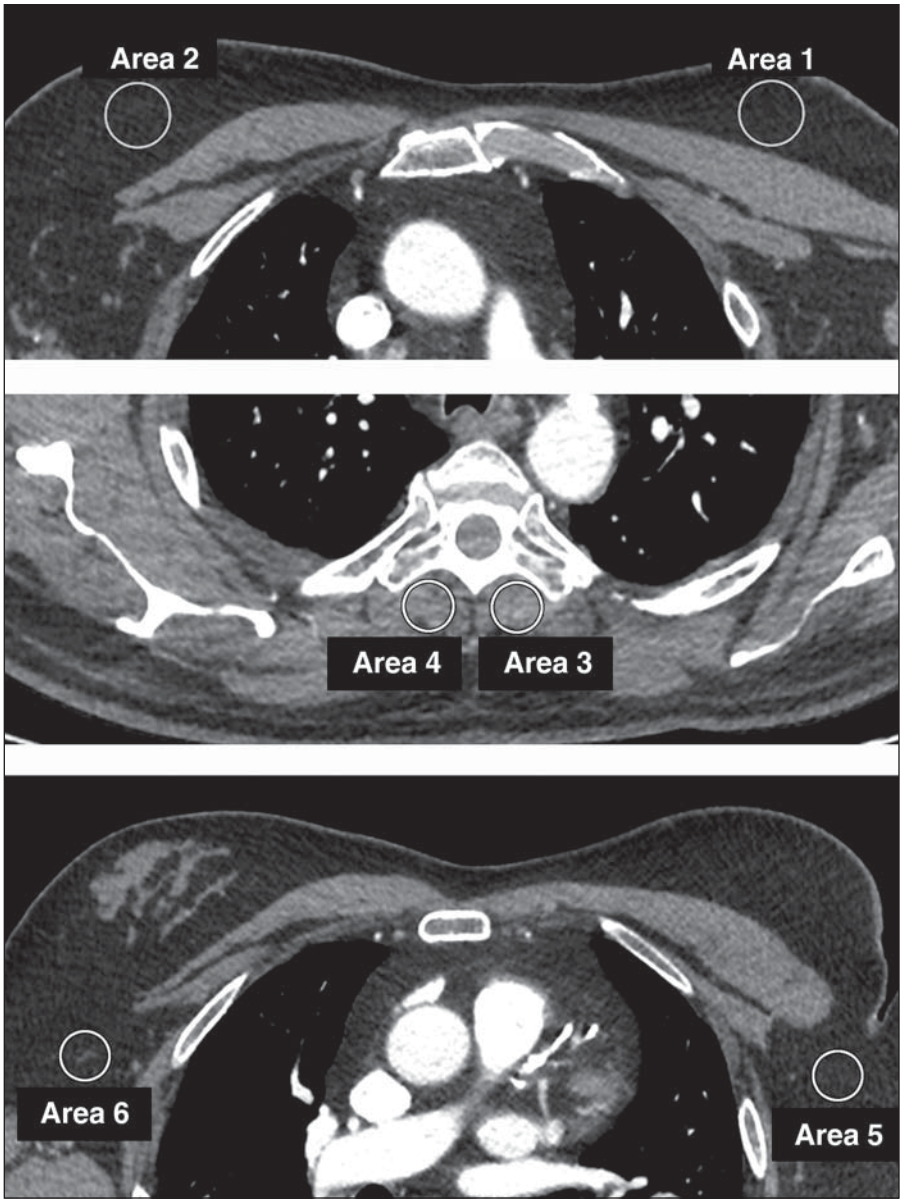

Fig. 2—Measurements of region of interests (ROIs) for objective analysis. Six areas were measured with circular ROIs. Area 1 is subcutaneous fat within anterior left chest, area 2 is subcutaneous fat within anterior right chest, area 3 is paraspinal muscle left, area 4 is paraspinal muscle right, area 5 is subaxillary fat left, and area 6 is subaxillary fat right.

also allowed to change the window level, width, and magnification as per their comfort level during assessment. The purpose of our study was to ascertain whether the low-dose scans reconstructed with MBIR were of diagnostic quality and were not inferior to our standard-of-care scan reconstructed using ASIR with 30% blending at NI 33. The following parameters were assessed with binary ratings (0 = nondiagnostic or inferior, and 1 = diagnostic or superior) as compared with standard-of-care scans: subjective image quality, subjective image noise, delineation of normal lung markings and visibilities of small structures (i.e., lung markings and small vessels in peripheral 2 cm of the lungs), artifacts, and overall diagnostic confidence in the study. Where there were pathologic abnormalities, subjective visual lesion conspicuity was also assessed.

Radiation Dose

For each patient, dose-length products (DLPs) were recorded. Effective dose (ED) was calculated for each NI using a conversion factor of 0.014 taken from a normalized value of ED per DLP for chest [12].

Statistical Analysis

Data were analyzed by using statistical software (Prism version 5.0d, GraphPad Software). Quantitative data such as objective image noise and mean attenuation were analyzed by comparing SDs and 95% CIs. Mean image noise values and attenuation values were compared between different reconstruction algorithms using repeated-measures analysis of variance with Dunnette posttesting for multiple comparisons, with ASIR at NI of 33 used as a control. Mean differences in image noise between FBP at NI 33, ASIR at NI 33, and MBIR at NIs 60 and 70 were compared for significance using paired Student *t* tests. Significance is defined as a p value less than 0.05.

Qualitative data were assessed as follows. The interobserver agreement between the two radiologists for each of the assessed subjective image quality and lesion assessment parameters was estimated by using weighted kappa statistics. Definitions of levels of interobserver agreement on the basis of kappa values was classified as follows: poor, 0–0.20; fair, 0.21–0.40; moderate, 0.41–0.60; good, 0.61–0.80; and excellent, 0.81–1.0. Percentages of diagnostic acceptability for individual parameters were also calculated.

Results

Objective Image Quality Assessment

A summary of image noise and mean CT numbers across all nine datasets among the three different reconstruction methods are summarized in Table 1 as an average across all six regions. For each region, differences between the nine different algorithms show similar trends. Figure 3 is a graphical illustration of the trend for the region of subcutaneous fat (right). Paired Student *t* tests were performed between six different sampled regions individually comparing ASIR at NI 33 with either MBIR at NI 60 or MBIR at NI 70 and show significant differences between means ($p < 0.001$).

Mean attenuation differences across nine different reconstruction algorithms were analyzed using repeated-measures analysis of variance with Dunnette posttest for multiple comparison using ASIR at NI 33 as a control. There was no significant change in the mean CT numbers between different reconstructions ($p > 0.05$). Figure 4 illustrates differences in mean attenuation in subaxillary fat (left). Individual averages of noise and attenuation values of six anatomic regions measured are summarized in Appendix 1.

Subjective Lesion and Image Quality Assessment

Overall, there was good agreement between the two observers in rating of image noise (κ =

TABLE 1: Image Noise, Averaged Across Six Different Anatomic Regions, Using Three Different Reconstruction Techniques at Three Different Noise Indexes

Reconstruction Technique	Noise Index 33	Noise Index 60	Noise Index 70
Filtered back projection	26.9 ± 7.7	45.6 ± 14.4	51.8 ± 15.6
Adaptive statistical iterative reconstruction (with 30% blending)	23.6 ± 6.8	38.6 ± 12.6	43.5 ± 13.4
Model-based iterative reconstruction	15.9 ± 4.8	18.4 ± 5.4	19.2 ± 5.6

Note—Data are mean ± SD.

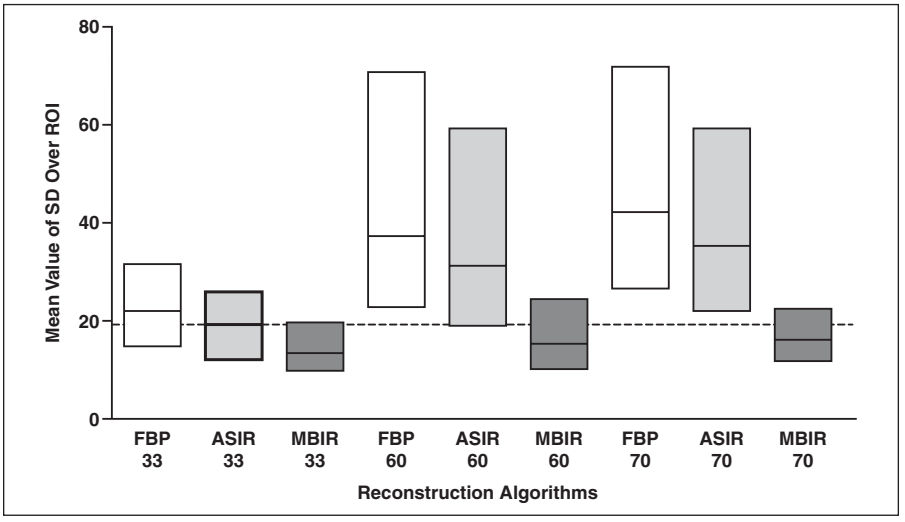

Fig. 3—Image noise in subcutaneous fat in right chest. Bars indicate maximum-to-minimum ranges at either end. Middle line indicates mean. Dashed line represents mean for adaptive statistical iterative reconstruction (ASIR) at noise index 33 for comparison. Numbers on *x*-axis indicate noise index setting for each algorithm. FBP = filtered back projection, MBIR = model-based iterative reconstruction, ROI = region of interest.

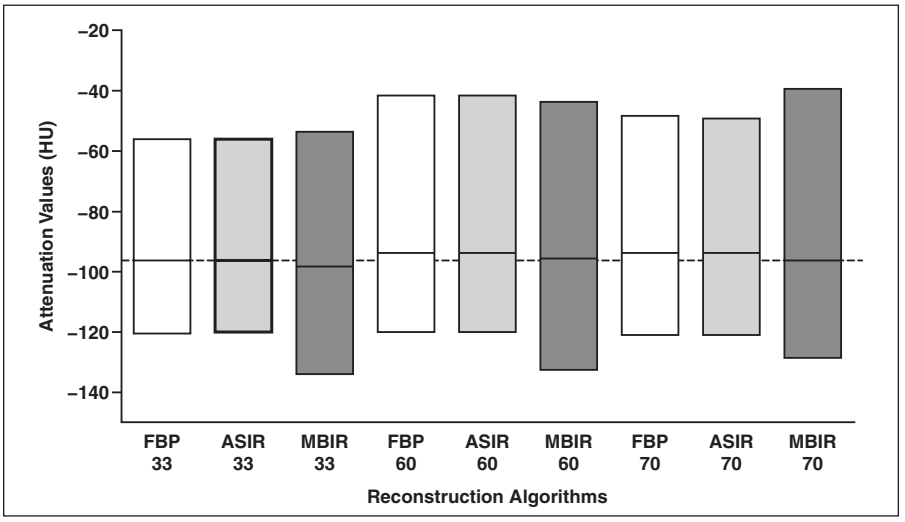

Fig. 4—Attenuation value averages for left subaxillary fat. Bars indicate maximum-to-minimum ranges at either end. Middle line indicates mean. Dashed line represents mean for adaptive statistical iterative reconstruction (ASIR) at noise index 33 for comparison. Numbers on *x*-axis indicate noise index setting for each algorithm. FBP = filtered back projection, MBIR = model-based iterative reconstruction.

0.795). There was excellent-to-complete agreement in delineation of anatomic structures (κ = 1), conspicuity of lesions (κ = 1), artifacts (κ = 0.843), and overall diagnostic quality of the study (κ = 1). Percentages of overall diagnostic confidence were 97% for FBP at NI 33 and 100% for ASIR at NI 33 and MBIR at NIs 60 and 70. For each parameter of noise, contrast, anatomic delineation, and lesion conspicuity, the diagnostic acceptability was 100% for all four reconstruction algorithms.

A total of 64 lesions were assessed. These included lung nodules (*n* = 24), lymph nodes (*n* = 9), bullae (*n* = 3), pleural thickening (*n* = 2), streaky shadowing (*n* = 4), bronchioles thickening (*n* = 1), fibrosis (*n* = 1), pleural fluid or effusion (*n* = 4), thyroid nodule (*n* = 1), pleural metastases (*n* = 8), vertebral collapse (*n* = 1), vertebral metastases (*n* = 4), rib fracture (*n* = 1), and mitral valve calcification (*n* = 1). Specific analysis of lung nodules revealed complete interobserver agreement (κ = 1) with 100% of scores of diagnostic quality. Specific analysis of soft-tissue structures (lymph nodes, pleural thickening, thyroid nodule, and pleural fluid, effusion, or metastases) reveals excellent interobserver agreement (κ = 0.84) with percentages of diagnostic acceptability as follows: 87% for FBP at NI 33 and 100% each for ASIR at NI 33 and MBIR at NIs 60 and 70.

A total of 13 artifacts were also assessed, including streak artifacts due to metals and leads, beam-hardening artifacts due to arms by body side or large body size, truncation artifacts, streaky artifacts due to prosthesis, photon starvation, zebra artifact, and streak artifacts due to contrast medium. Artifact was deemed acceptable in 62% of cases for FBP at NI 33, 69% of cases for ASIR at NI 33, and 100% of cases for MBIR at NIs 60 and 70. Percentages of diagnostic acceptability are listed in Table 2.

Radiation Doses

Average radiation doses (DLPs and EDs) are summarized in Table 3. EDs were 3.7, 1.2, and 0.9 mSv for standard scan (NI 33), NI 60, and NI 70, respectively (Table 3). In our study, the DLP and ED for standard-dose CT (247.3 mGy × cm; 3.7 mSv) were already lower than the typical doses described in the National Radiological Protection Board's report [12] for chest CT examinations of adults with a mean weight of about 70 kg (400 mGy × cm; 5.6 mSv). The ED for low-dose CT (0.9 mSv) was marginally lower than the average ED for

TABLE 2: Diagnostic Acceptability

Lesion	Filtered Back Projection at Noise Index 33	Adaptive Statistical Iterative Reconstruction at Noise Index 33	Model-Based Iterative Reconstruction at Noise Index 60	Model-Based Iterative Reconstruction at Noise Index 70
Lung nodule (n = 24)	100	100	100	100
Soft-tissue lesion (n = 15)	87	100	100	100
Artifact (n = 13)	62	69	100	100

Note—Data are percentage diagnostic acceptability.

TABLE 3: Dose-Length Product (DLP) and Effective Dose for Each Noise Index

Noise Index	DLP (mGy × cm)	Effective Dose (mSv)
33	247.3 ± 154.4	3.7 ± 2.3
60	83.2 ± 55.3	1.2 ± 0.8
70	61.6 ± 41.2	0.9 ± 0.6

Note—Data are average ± SD.

low-dose CT described by the National Lung Screening Trial (1.4 mSv) [13]. We recognize that using DLP-based methods for calculation underestimates the ED as compared with organ dose estimates based on tissue-weighting factors (e.g., 23% difference from the International Commission on Radiological Protection's report 60) [14].

Discussion

With increasing use of CT, awareness of radiation dose is important, as well as making the best use of novel technologies that can reduce radiation burden. This study aims to evaluate the role of MBIR compared with other CT reconstruction algorithms.

Iterative reconstruction as a concept has been around since the very first CT scanners, which originally used a type of iteration known as the algebraic reconstruction algorithms, which use mathematic "trial and improvement" repetitions that gradually converge to the correct pixel value in question. Because several iterations are often required to obtain a satisfactory image (which is more time consuming), this technique was too slow for use in CT where algebraic reconstruction algorithms demanded a mathematic solution to a 512 × 512 pixel dataset. It was quickly superseded by the so-called analytical reconstruction technique, FBP, which is now routinely used in modern CT systems. FBP is robust and relatively undemanding on computer processing. It is still widely used today and is considered acceptable for clinical diagnosis, but it does not provide optimal results for depiction of the patient because it makes many incorrect assumptions about the data. This is apparent in the inherent level of artifacts and noise in FBP images.

ASIR is a postprocessing reconstruction method recently marketed by GE Healthcare, where the starting solution is assumed from FBP and corrected iteratively using a basic optical model improved by accounting for measurement statistics. The level of ASIR iteration applied can be blended with the starting solution (FBP) to a level consistent with the diagnostic requirements.

MBIR represents a new reconstruction method wherein the limitations of FBP are abandoned altogether. The system model is complex, allowing a finite (known) source, image voxel, and detector. By knowing the actual dimensions of the x-ray source (anode) and the detector response function, we can better simulate our photon optics (simulation of x-ray paths) and reduce the error in image reconstruction. A forward projection is performed on an assumed starting image. Datasets from the system model are compared with the acquired dataset,

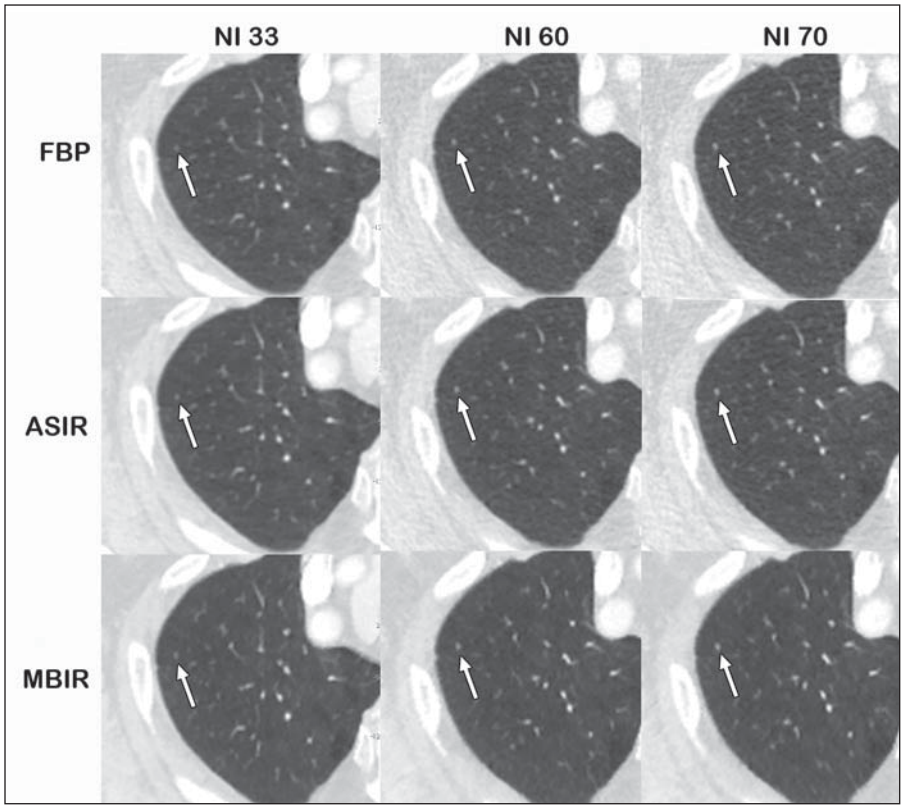

Fig. 5—65-year-old man with known diagnosis of cholangiocarcinoma. Transverse chest CT images show small lung nodule reconstructed with different algorithms as shown. Note that even submillimeter lung nodule as in this case is well seen across all reconstruction algorithms because of inherent high contrast of air to soft tissue nodule. ASIR = adaptive statistical iterative reconstruction, FBP = filtered back projection, MBIR = model-based iterative reconstruction, NI = noise index.

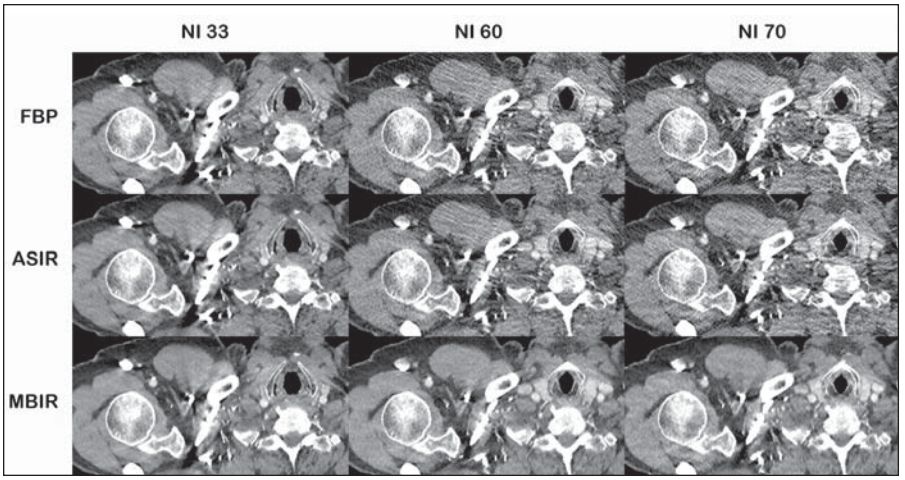

Fig. 6—73-year-old woman undergoing CT for follow-up breast cancer surveillance. Transverse chest CT images show soft-tissue structures in upper chest. Note noisier images with filtered back projection (FBP) and adaptive statistical iterative reconstruction (ASIR) compared with model-based iterative reconstruction (MBIR). NI = noise index.

and the model input image is adjusted until convergence criteria are met. With a more accurate representation of system optics, and utilizing forward projection models, image noise can be significantly reduced when compared with FBP. Some authors have reported dose reductions of up to 80% of those required for FBP [15]. The disadvantage of MBIR is the computing power required. Computers had to be built specifically to handle this task. Currently, the processing time of the images are still significantly slower than traditional techniques (approximately 45 minutes per series), although the actual scanning time for the patient remains the same. However, it has the potential to perform CT scans at substantially reduced doses, thus significantly shifting the risk-to-benefits ratio very much in favor of CT.

What we have shown in this study confirms the feasibility of using MBIR as a new reconstruction algorithm in clinical practice. Even when we scanned at the lowest doses (submillisievert in many cases), objective measurements were superior to those using traditional reconstruction methods. Over six anatomic areas, mean image noise for MBIR at NIs 60 and 70 were lower than that of ASIR at NI 33, which is our current standard-of-care scan ($p < 0.05$). The mean average attenuation values for MBIR at NIs 60 and 70 were 1.7 and 1.6 HU, respectively, for combined subcutaneous fat and 2 HU higher for combined paraspinal muscles than that of ASIR at NI 33, although the differences were not statistically significant ($p > 0.05$). Marked differences in attenuation values between FBP scanning at NIs 60 and 70, compared with ASIR, are to be expected because of the noisier images. This slight alteration is consistent with mean CT number as measured with phantom sensitometry (Catphan, Southern Scientific) testing in our own center and also in the literature [15]. Subjective assessment did not reveal a statistical difference in the perception of image noise. More important, overall diagnostic confidence for the study remains at 100%, even for low-dose MBIR images.

The objective of our study was not to see how the MBIR algorithm could improve image quality but rather to establish whether MBIR used at a low dose can achieve images with diagnostic quality similar to that of our standard-of-care scan (ASIR with 30% blending at NI 33). This is the reason we have deviated from using the traditional scoring criteria using a 4- or 5-point Likert scale [16]. Instead, we opted to use a binary scale using parameters similar to that of the European Guidelines on quality criteria for CT [16]. We have shown that there is good-to-excellent agreement between two observers, with extremely high diagnostic acceptability (97–100%). Higher acceptability for artifacts at lower NIs with MBIR is an interesting observation, which can be attributed, in part, to fewer beam-hardening artifacts. Some side-by-side comparisons of scans of comparing image quality and common pathologic abnormalities are shown as examples (Figs. 5–7).

For all lesions assessed, the low-dose images were shown to be as good as the normal-dose images for diagnostic quality. The MBIR images do look different, however, but we have shown that diagnostic confidence was not affected in our limited assessment for lung nodule detection and soft-tissue structures. Lesions such as lung nodules are commonly encountered in clinical practice, and low-dose scanning has significant bearing, especially for its use in the context of lung nodule surveillance and, increasingly, as a screening tool for lung cancer [17–20]. Significant dose savings can be achieved (an average of 76% reduction if an NI of 70 is used; Table 2), but its diagnostic accuracy in the routine clinical practice should be further assessed with larger sample. Although we did not assess for this specifically, detection and characterization of lung nod-

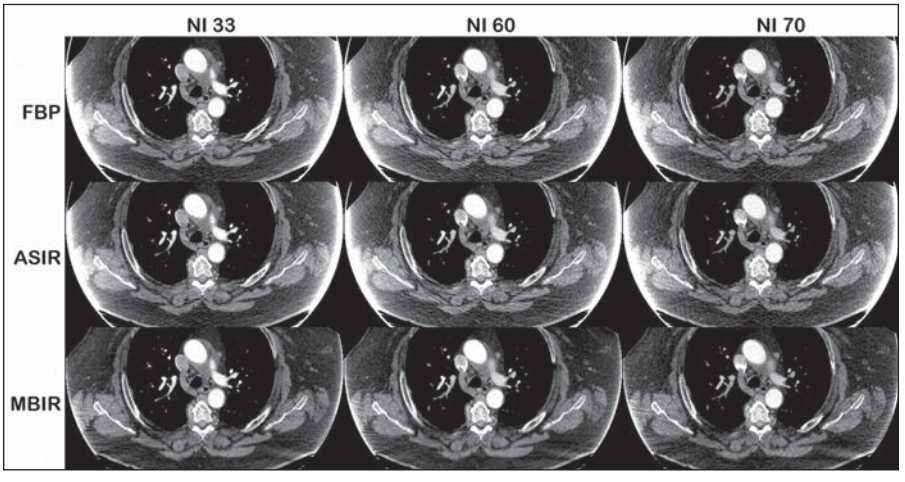

Fig. 7—67-year-old woman undergoing CT for follow-up of treated lymphoma. Transverse chest CT images show small volume mediastinal lymphadenopathy reconstructed with different algorithms as shown. Note that edge artifacts related to patient's size are significantly reduced with model-based iterative reconstruction (MBIR). ASIR = adaptive statistical iterative reconstruction, FBP = filtered back projection, NI = noise index.

ules in our preliminary study do appear to be equivalent for FBP, ASIR, and MBIR, even at low doses (Fig. 5). This is likely because there is inherently high contrast difference between lung nodule and the surrounding lung. In our limited analysis of soft-tissue lesions, MBIR at NIs 60 and 70 do appear to show diagnostic equivalence (diagnostic acceptability of 100%) to ASIR at NI 33 and are superior to FBP at NI 33 (diagnostic acceptability of 87%). There also appear to be benefits in artifact reduction (Fig. 7), with diagnostic acceptabilities of 100% for MBIR, 69% for ASIR, and 62% for FBP. Because our sample sizes for lesions were small (e.g., $n = 24$ for lung nodules, $n = 15$ for soft tissue lesions, and $n = 13$ for artifacts), we did not think that robust analysis could be performed across all available reconstruction methods. A larger sample size with more lesions would be required.

There are limitations to our study. First, this is a limited study comprising 30 patients. Second, the indications for scanning our patients were for oncologic surveillance, and scans were performed sequentially using an IV contrast agent. Therefore, the structures in the mediastinum and the lungs were affected by differential contrast opacification. For this reason, we did not assess specifically the contrast and contrast-to-noise ratio of various structures. Although differential contrast opacification could affect image quality, this effect has been reduced as far as possible by minimizing the delay between the scans and also by altering the order at which the low-dose scans were performed. Sequential scans are also susceptible to movement. Attempts are always made when performing objective analysis to line up the slices as closely as possible to compensate for different patient positions when this has occurred.

Third, our patients have different pathologic abnormalities, and although we have shown that nodule detection was diagnostically acceptable, the numbers are still too few for adequate accuracy assessment. Other specific pathologic abnormalities, such as ground-glass opacification or features of diffuse lung disease (e.g., honeycombing or fine reticulations), were not specifically assessed. More patients with these specific pathologic entities are required to assess the accuracy and feasibility of this new method in these specific settings. In this preliminary study, it appears that MBIR provides significant advantages in a low-dose setting in assessing soft-tissues structures and artifact reduction; however, reviewing lesions that have inherent high contrast (e.g., lung nodule detection or characterization) may be possible for traditional reconstruction such as FBP even at a low dose. Subjective comparisons among all three reconstructions and at all dose levels with more lesions will allow more informative conclusion to be reached, and this needs to be further explored.

In conclusion, MBIR shows superior noise reduction even at low doses. Substantial dose reduction can be achieved by increasing the NI as tested in this study without affecting image quality or diagnostic confidence. MBIR offers yet another tool in the radiology armory against this increasing trend and concern.

References

1. Mettler FA, Bhargavan M, Faulkner K, et al. Radiologic and nuclear medicine studies in the United States and worldwide: frequency, radiation dose, and comparison with other radiation sources—1950–2007. *Radiology* 2009; 253:520–531
2. United Nations. Report of the United Nations Scientific Committee on the Effects of Atomic Radiation 2010, 57th session: includes scientific report—summary of low-dose radiation effects on health. United Nations Publications website. unp.un.org/Details.aspx?pid=22259. Published 2011. Accessed October 23, 2012
3. Hart D, Wall BF, Hillier MC, Shrimpton PC. *Frequency and collective dose for medical and dental x-ray examination in the UK, 2008.* London, UK: Health Protection Agency, 2010:52
4. Singh S, Kalra MK, Gilman MD, et al. Adaptive statistical iterative reconstruction technique for radiation dose reduction in chest CT: a pilot study. *Radiology* 2011; 259:565–573
5. Singh S, Kalra MK, Hsieh J, et al. Abdominal CT: comparison of adaptive statistical iterative and filtered back projection reconstruction techniques. *Radiology* 2010; 257:373–383
6. Cornfeld D, Israel G, Detroy E, Bokhari J, Mojibian H. Impact of adaptive statistical iterative reconstruction (ASIR) on radiation dose and image quality in aortic dissection studies: a qualitative and quantitative analysis. *AJR* 2011; 196:713; [web]W336–W340
7. Yanagawa M, Honda O, Yoshida S, et al. Adaptive statistical iterative reconstruction technique for pulmonary CT: image quality of the cadaveric lung on standard- and reduced-dose CT. *Acad Radiol* 2010; 17:1259–1266
8. Sagara Y, Hara AK, Pavlicek W, et al. Comparison of low-dose CT with adaptive statistical iterative reconstruction and routine-dose CT with filtered back projection in 53 patients. *AJR* 2010; 195:713–719
9. Marin D, Nelson RC, Schindera ST, et al. Low-tube-voltage, high-tube-current multidetector abdominal CT: improved image quality and decreased radiation dose with adaptive statistical iterative reconstruction algorithm—initial clinical experience. *Radiology* 2010; 254:145–153
10. Pontana F, Duhamel A, Pagniez J, et al. Chest computed tomography using iterative reconstruction vs filtered back projection. Part 2. Image quality of low-dose CT examinations in 80 patients. *Eur Radiol* 2011; 21:636–643
11. Pontana F, Pagniez J, Flohr T, et al. Chest computed tomography using iterative reconstruction vs filtered back projection. Part 1. Evaluation of image noise reduction in 32 patients. *Eur Radiol* 2011; 21:627–635
12. Shrimpton PC, Hillier MC, Lewis M, Dunn M. *NRPB report W67: doses from computed tomography (CT) examinations in the UK—2003 review.* London, UK: National Radiological Protection Board, 2005
13. Larke FJ, Kruger RL, Cagnon CH, et al. Estimated radiation dose associated with low-dose chest CT of average-size participants in the National Lung Screening Trial. *AJR* 2011; 197:1165–1169
14. Christner JA, Kofler JM, McCollough CH. Estimating effective dose for CT using dose–length product compared with using organ doses: consequences of adopting International Commission on Radiological Protection Publication 103 or dual-energy scanning. *AJR* 2010; 194:881–889
15. Miéville FA, Gudinchet F, Brunelle F, Bochud FO, Verdun FR. Iterative reconstruction methods in two different MDCT scanners: physical metrics and 4-alternative forced-choice detectability experiments—a phantom approach. *Phys Med* 2012 Jan 2 [Epub ahead of print]
16. Leonardi M, Bongartz G, Geleijns DJ, et al. European guidelines on quality criteria for computed tomography. European Commission website. w3.tue.nl/fileadmin/sbd/Documenten/Leergang/BSM/European_Guidelines_Quality_Criteria_Computed_Tomography_Eur_16252.pdf. Published 1999. Accessed October 23, 2012
17. Menezes RJ, Roberts HC, Paul NS, et al. Lung cancer screening using low-dose computed tomography in at-risk individuals: the Toronto experience. *Lung Cancer* 2010; 67:177–183
18. Kramer BS, Berg CD, Aberle DR, Prorok PC. Lung cancer screening with low-dose helical CT: results from the National Lung Screening Trial (NLST). *J Med Screen* 2011; 18:109–111
19. Bowman RV, Crossin J, Courtney D, et al. The Queensland Lung Cancer Screening Study: rationale, design and methods. *Intern Med J* 2012 Apr 4 [Epub ahead of print]
20. Aberle DR, Berg CD, Black WC, et al.; National Lung Screening Trial Research Team. The National Lung Screening Trial: overview and study design. *Radiology* 2011; 258:243–253

(Appendix follows on next page)

APPENDIX 1: Averages of Noise and Attenuation Values

Tables 4 and 5 show individual averages of noise and attenuation values of six anatomic regions measured. Area 1 includes subcutaneous fat within the anterior left chest, area 2 includes the subcutaneous fat within the anterior right chest, area 3 is the left paraspinal muscle, area 4 is the right paraspinal muscle, area 5 is the left subaxillary fat, and area 6 is the right subaxillary fat.

TABLE 4: Image Noise per Anatomic Area Across Nine Different Series

Reconstruction Technique, Noise Index	Area 1	Area 2	Area 3	Area 4	Area 5	Area 6
Filtered back projection						
33	23.2 ± 4.3	22.0 ± 3.8	33.4 ± 8.4	32.3 ± 9.1	26.3 ± 5.5	24.5 ± 5.7
60	38.7 ± 8.8	37.4 ± 10.7	58.7 ± 17.8	55.9 ± 12.7	42.8 ± 8.1	40.2 ± 8.1
70	43.9 ± 7.1	42.2 ± 9.8	66.4 ± 16.0	64.6 ± 18.1	48.6 ± 9.3	44.9 ± 8.5
Adaptive statistical iterative reconstruction						
33	20.2 ± 3.4	19.2 ± 3.3	29.1 ± 7.4	28.3 ± 8.1	23.3 ± 5.0	21.7 ± 5.4
60	32.7 ± 7.5	31.3 ± 8.9	49.9 ± 16.2	47.4 ± 12.2	36.5 ± 7.2	22.9 ± 6.9
70	36.7 ± 5.7	35.2 ± 8.1	55.8 ± 13.7	54.3 ± 16.3	41.1 ± 8.0	37.7 ± 7.2
Model-based iterative reconstruction						
33	14.4 ± 3.3	13.4 ± 2.6	17.8 ± 5.0	17.6 ± 5.1	16.6 ± 5.8	15.7 ± 5.1
60	16.4 ± 3.0	15.3 ± 3.0	20.7 ± 6.2	21.2 ± 6.0	18.9 ± 6.2	17.7 ± 4.5
70	17.1 ± 3.4	16.2 ± 3.0	21.7 ± 6.0	21.5 ± 5.7	20.8 ± 7.7	18.3 ± 4.1

Note—Data are mean ± SD.

TABLE 5: Attenuation Values per Anatomic Area Across Nine Different Series

Reconstruction Technique, Noise Index	Area 1	Area 2	Area 3	Area 4	Area 5	Area 6
Filtered back projection						
33	–109.5 ± 30.6	–111.4 ± 29.6	41.4 ± 14.7	40.6 ± 14.0	–96.5 ± 16.0	–101.4 ± 12.2
60	–108.8 ± 28.3	–108.4 ± 29.7	43.9 ± 17.2	42.8 ± 15.1	–94.1 ± 16.9	–99.7 ± 12.9
70	–109.8 ± 31.3	–109.9 ± 30.4	43.9 ± 18.1	42.8 ± 17.1	–93.7 ± 16.9	–100.3 ± 13.3
Adaptive statistical iterative reconstruction						
33	–109.3 ± 30.5	–111.3 ± 29.6	41.6 ± 14.8	41.0 ± 14.1	–96.3 ± 15.8	–101.2 ± 12.1
60	–108.5 ± 29.0	–108.7 ± 29.8	44.0 ± 17.2	42.8 ± 15.1	–94.0 ± 17.0	–99.6 ± 12.9
70	–109.9 ± 30.6	–110.0 ± 30.4	43.9 ± 18.1	42.8 ± 17.1	–93.7 ± 16.8	–100.3 ± 13.4
Model-based iterative reconstruction						
33	–107.1 ± 31.7	–109.2 ± 31.1	44.8 ± 14.6	42.9 ± 17.1	–98.3 ± 16.9	–100.9 ± 11.7
60	–108.2 ± 27.8	–108.5 ± 29.3	44.1 ± 14.7	42.5 ± 15.1	–95.7 ± 17.7	–99.0 ± 12.9
70	–108.2 ± 27.9	–108.0 ± 30.5	44.3 ± 14.6	42.3 ± 17.8	–96.1 ± 18.3	–99.3 ± 13.4

Note—Data are mean ± SD Hounsfield units.

FOR YOUR INFORMATION

This article is available for CME/SAM credit. To access the exam for this article, follow the prompts associated with the online version of the article.